# Effect of antiferromagnetic spin correlations on lattice distortion and charge ordering in $Pr_{0.5}Ca_{1.5}MnO_4$

Songxue Chi*, F. Ye†, Pengcheng Dai*†‡, J. A. Fernandez-Baca*†, Q. Huang§, J. W. Lynn§, E. W. Plummer*†‡, R. Mathieu¶, Y. Kaneko¶, and Y. Tokura¶‖

*Department of Physics and Astronomy, University of Tennessee, Knoxville, TN 37996-1200; †Oak Ridge National Laboratory, Oak Ridge, TN 37831-6393; §NIST Center for Neutron Research, National Institute of Standards and Technology, Gaithersburg, MD 20899-6102; ¶Spin Structure Project (ERATO), Japan Science and Technology Corporation, Advanced Industrial Science and Technology Central 4, Tsukuba 305-8562, Japan; and ‡Department of Applied Physics, University of Tokyo, Tokyo 113-8656, Japan

Contributed by E. W. Plummer, May 8, 2007 (received for review March 5, 2007)

**We use neutron scattering to study the lattice and magnetic structure of the layered half-doped manganite $Pr_{0.5}Ca_{1.5}MnO_4$. On cooling from high temperature, the system first becomes charge- and orbital-ordered (CO/OO) near $T_{CO} = 300$ K and then develops checkerboard-like antiferromagnetic (AF) order below $T_N = 130$ K. At temperatures above $T_N$ but below $T_{CO}$ ($T_N<T<T_{CO}$), the appearance of short-range AF spin correlations suppresses the CO/OO-induced orthorhombic strain, contrasting with other half-doped manganites, where AF order has no observable effect on the lattice distortion. These results suggest that a strong spin-lattice coupling and the competition between AF exchange and CO/OO ordering ultimately determines the low-temperature properties of the system.**

CE-type AF order

Understanding the competition and coupling between charge, lattice, and spin degrees of freedom in doped transition metal oxides continues to be one of the most profound intellectual challenges in modern condensed matter physics since the discovery of high-transition temperature (high-$T_c$) superconductors and the colossal magnetoresistance manganese oxides (1). The complexity of transition metal oxides is directly responsible for their tunability, and the balance between different competing phases can produce large changes in the physical properties. For example, superconductivity in the high-$T_c$ superconductors $La_{2-x}Ba_xCuO_4$ becomes drastically suppressed at the doping level of $x=1/8$ due to the spin and charge phase separation (the so-called "striped" phase), where charge ordering (CO) establishes a template at a higher temperature to be followed by antiferromagnetic (AF) stripe order at a lower temperature (2, 3). The low-temperature AF phase has little or no influence on the already established CO phase because of its low energy scales. Similarly, the long-range AF order in the parent compounds of high-$T_c$ copper oxides is characterized by spin-only antiferromagnetism and has little or no effect on the underlying lattice (1). These results suggest that spin-lattice coupling is weak in high-$T_c$ copper oxides.

In the case of colossal magneroresistance (CMR) manganites $A_{1-x}A'_xMnO_3$ (where $A$ and $A'$ are trivalent rare- and divalent alkaline-earth ions respectively), the competition between charge, lattice, and spin degrees of freedom can be delicately balanced to form a variety of ground states (1). Before doping any holes into the system, the parent compound such as $LaMnO_3$ has an insulating ground state, where the $Mn^{3+}$ spins order in the A-type AF structure (4, 5). For hole-doping level around $x = 0.3$ by substituting trivalent $La^{3+}$ with divalent $Ca^{2+}$, $La_{1-x}Ca_xMnO_3$ becomes a metallic ferromagnet with a CMR effect near the Curie temperature $T_C$. The formation of long-range ferromagnetic order at $T_C$ also induces a large lattice distortion, suggesting a strong spinlattice coupling (6). Upon increasing the doping level to $x=0.5$, $La_{0.5}Ca_{0.5}MnO_3$ changes again into an AF insulating phase but with a CE-type AF structure (4). Here, equal amounts of $Mn^{3+}$ and $Mn^{4+}$ distribute alternately in the $MnO_2$ plane of $La_{0.5}Ca_{0.5}MnO_3$, forming a checkerboard CE-type pattern as schematically depicted in Fig. 1*a* (4, 5). Although the CE-type AF order disappears on warming above the Néel temperature $T_N$, the system is still charge and orbitally ordered (CO/OO). Such CO/OO order is strongly coupled to the lattice and induces an orthorhombic distortion that only disappears at temperatures well above the CO/OO ordering temperature $T_{CO}$.

For example, in the three-dimensional nearly half-doped perovskites $La_{0.5}Ca_{0.5}MnO_3$ (7), $Pr_{0.5}Ca_{0.5}MnO_3$ (8, 9), and $Pr_{0.55}(Ca_{0.8}Sr_{0.2})_{0.45}MnO_3$ (10), the CO/OO-ordered lattice first established slightly below room temperature is followed by a CE-type AF order around 130 K (Fig. 1*a*). X-ray and neutron diffraction experiments have shown that the materials exhibit a tetragonal to orthorhombic phase transition near $T_{CO}$. Furthermore, the orthorhombicity increases with decreasing temperature and shows no anomalies across the CE-type AF phase transition (7–10). These results thus suggest that CO/OO order is strongly coupled to the lattice and there is a weak spin-lattice coupling. As a consequence, CO/OO ordering in half-doped perovskites may have a larger energy scale than the low temperature magnetic order. For the single layer half-doped manganites such as $La_{0.5}Sr_{1.5}MnO_4$ (LSMO), a similar behavior is also observed. Here, the material exhibits a tetragonal to orthorhombic phase transition at the CO/OO temperature of 230 K and then orders antiferromagnetically with a CE-structure below ≈120 K (11, 12). The lattice distortion and orthorhombicity of LSMO show no anomalies below the AF phase transition. Therefore, it appears that CO/OO order in doped transition metal oxides generally is strongly coupled to the lattice, whereas the low-temperature magentic order has no influence on CO/OO ordering.

Although CO/OO order in doped manganites may have a stronger coupling to the lattice than that of the AF order, its microscopic origin is still unclear. Theoretically, CO/OO order established at higher temperatures may actually have a purely

Author contributions: S.C., F.Y., and P.D. designed research; S.C., F.Y., J.A.F.-B., Q.H., and J.W.L. performed research; Y.K. and Y.T. contributed new reagents/analytic tools; R.M. analyzed data; and S.C., P.D., and E.W.P wrote the paper.

The authors declare no conflict of interest.

Freely available online through the PNAS open access option.

Abbreviations: LMSO, $La_{0.5}Sr_{1.5}MnO_4$; PCMO, $Pr_{0.5}Ca_{1.5}MnO_4$; CO/OO, charge and orbitally ordered.

‡To whom correspondence may be addressed. E-mail: daip@ornl.gov or eplummer@utk.edu.

This article contains supporting information online at www.pnas.org/cgi/content/full/0704303104/DCI.

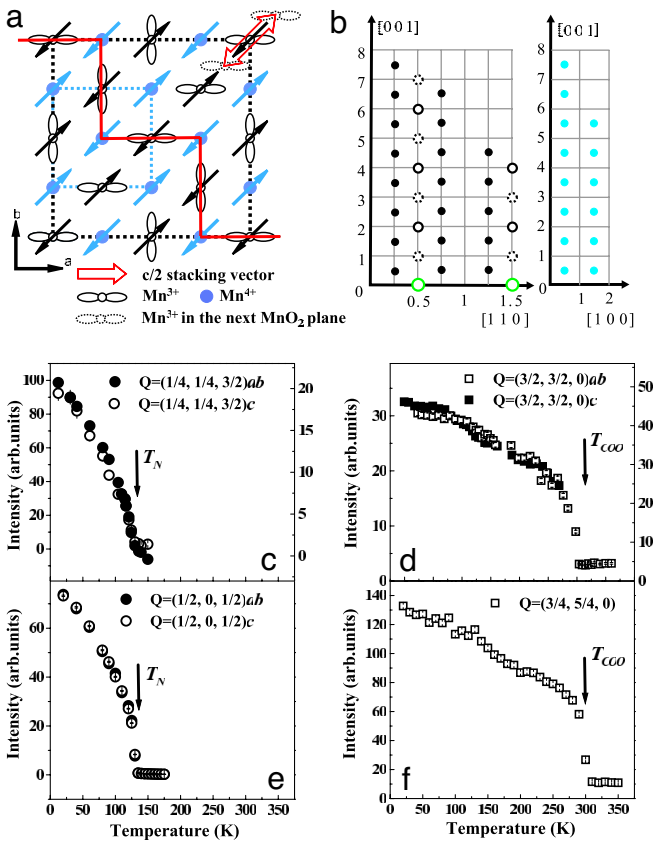


**Fig. 1.** Structural scatterings and their temperature dependence. (*a*) Schematic view of the CE-type AF ordering in the $MnO_2$-plane. The black dashed line represents the periodicity of the unit cell for the $Mn^{3+}$ sublattice, and the blue dashed line shows that of the $Mn^{4+}$ sublattice. Possible spin arrangements in the *c*/2 stacking layers are marked by red arrows. The directions of $Mn^{3+}$ orbitals form zigzag ferromagnetic chains (red line) that order antiferromagnetically. (*b*) The observed nuclear peaks (black open circles), CO/OO-induced superlattice peaks (green open circles) and magnetic ordering (solid circles) in reciprocal space. The dotted open circles represent the observed weak nuclear peaks that are disallowed by orthorhombic symmetry, indicating that the symmetry is lower than orthorhombic. Temperature dependence of the AF peak intensity from (1/4, 1/4, 3/2) (*c*) and (1/2, 0, 1/2) (*e*) and temperature dependence of CO/OO peak intensity from (3/2, 3/2, 0) (*d*) and (3/4, 5/4, 0) (*f*) are shown.

magnetic spin origin (13); arise from a competition between the kinetic energy of the electrons and the magnetic exchange energy (14), due to a tendency of the Jahn–Teller distorted $Mn^{3+}$ ions to maximize their relative distances to gain electron kinetic energy (15), or come from a purely Coulomb interaction without invoking magnetic interactions (16, 17). In general, charge ordering in half-doped manganites is intimately related to the orbital ordering, where the orbitals of $e_g$ electrons on $Mn^{3+}$ sites form zigzag ferromagnetic chains that order antiferromagnetically (Fig. 1*a*) (18, 19). One way to sort out the relationship between CO/OO and CE-type AF order is to carry out systematic measurements on $A_{0.5}A'_{0.5}MnO_3$ or layered $A_{0.5}A'_{1.5}MnO_4$ with different $A$ and $A'$ ionic sizes. Decreasing the ionic size at $A$ and $A'$ sites in half-doped manganites increases the buckling of the $MnO_6$ octahedra and therefore the lattice distortion of the perovskite. For three-dimensional $A_{0.5}A'_{0.5}MnO_3$, replacing Sr in $Pr_{0.5}Sr_{0.5}MnO_3$ ($T_{CO}$ = 150 K) by the smaller Ca to form $Pr_{0.5}Ca_{0.5}MnO_3$ ($T_{CO}$ = 260 K) moderately enhances the CO/OO ordering temperature, but dramatically increases the magnitude of the magnetic field (from 5 T for $Pr_{0.5}Sr_{0.5}MnO_3$ to 27 T for $Pr_{0.5}Ca_{0.5}MnO_3$) needed to suppress CO/OO (20). These results suggest that CO/OO ordering is more stable for manganites with smaller ionic size and larger lattice distortion, and has an energy scale larger than that of the magnetic exchange. Because single crystals of three-dimensional $A_{0.5}A'_{0.5}MnO_3$ with the CE-type AF structure are unavailable, we study $A_{0.5}A'_{1.5}MnO_4$ with different $A$ and $A'$ ionic sizes.

## Results

Here, we present neutron scattering results on $Pr_{0.5}Ca_{1.5}MnO_4$ (PCMO), a single layer manganite with smaller average $A$ and $A'$ site ionic radius and larger lattice distortion than that of LSMO (the average $A$-site ionic radius for LSMO is $r_{ave}$ = 1.2865 Å, whereas it is $r_{ave}$ = 1.1798 Å for PCMO). We chose to study PCMO in order to determine the effect of the lattice distortion on the CO/OO and AF phase transitions. Because CO/OO is not affected by CE-type AF order in LSMO (11, 12), one would expect that CO/OO becomes more robust when the larger (La,Sr) ions in LSMO are replaced by smaller (Pr,Ca) in PCMO. Surprisingly, we find that the development of short-range AF spin correlations in the $MnO_2$ plane of PCMO significantly affects the CO/OO-induced lattice distortion and reduces the orthorhombicity of the system below $T_N$. Our results thus indicate the presence of a strong spin-lattice interaction, suggesting that antiferromagnetism can reduce the CO/OO-induced orthorhombic strain and thus compete with the CO/OO ordering.

We grew single crystals of PCMO using the traveling solvent floating zone technique. At room temperature, PCMO has the orthorhombic structure with lattice parameters $a_o$ = 5.380 Å, $b_o$ = 5.404 Å, and $c_o$ = 11.831 Å (space group *bmab*). For simplicity, we use the tetragonal unit cell for the triple-axis measurements and label the momentum transfers $\mathbf{q} = (q_x, q_y, q_z)$ as $(h, k, l) = (q_x a/2\pi, q_y a/2\pi, q_z c/2\pi)$ in reciprocal lattice units (rlu), where $a = (a_o + b_o)/2\sqrt{2}$ = 3.814 Å.

Because one expects PCMO to behave similarly to LSMO, we first probe the low-temperature magnetic and superlattice peaks associated with the CE-type AF structure and CO/OO state. Fig. 1 *d* and *f* shows the temperature dependence of the $\mathbf{q}$ = (3/2, 3/2, 0) and $\mathbf{q}$ = (3/4, 5/4, 0) structural superlattice peaks, respectively. Below ≈310 K, a structural phase transition associated with the CO/OO ordering occurs, consistent with the large increase in resistivity from transport measurements (21). Fig. 1 *c* and *e* shows the temperature dependence of the AF Bragg peaks at $\mathbf{q}$ = (1/4, 1/4, 3/2) and $\mathbf{q}$ = (1/2, 0, 1/2), corresponding to the $Mn^{3+}$ and $Mn^{4+}$ of the CE-type AF structure in Fig. 1*a*, respectively. The system develops AF order below 130 K, consistent with the results of bulk transport measurements (25) and similar to other half-doped manganites (4, 7–12).

To determine the low-temperature magnetic structure of PCMO, we made extensive surveys of reciprocal space and found that the allowed magnetic peaks are characterized by wavevectors $\mathbf{q} = (2n+1/4, 2n+1/4, l)$ and $(2n+1/2, 0, l)$ with $n$ and $l$ being integers and half-integers, respectively (Fig. 1*b*). Fig. 2 summarizes scans along the $l$ direction for the $(2n+1/4, 2n+1/4, l)$ (corresponding to the $Mn^{3+}$ sites) and $(2n+1/2, 0, l)$ (the $Mn^{4+}$ sites) Bragg positions. The $l = m+1/2$ ($m$ = 0, 1, 2, . . .) peaks are clearly magnetic because they disappear above the Néel temperature (Fig. 2*c*). We note that the *c*-axis correlation length in PCMO is resolution-limited and long-ranged, in contrast to the short-range *c*-axis correlations in LSMO (11). Magnetic structure factor calculations indicate two possible spin stackings of successive $MnO_2$ layers along the *c*-axis direction. As depicted in Fig. 1*a*, spins in the *c*/2 $MnO_2$ layer simply shift from those in the $c$ = 0 layer by $(a/2, a/2, c/2)$ or $(-a/2, -a/2, c/2)$. The stacking arrangements of $Mn^{3+}$ sublattice are also shown in Fig. 2*a*. The resulting magnetic structure allows both $(2n+1/4, 2n+1/4, l)$ and $(2n+1/2, 0, l)$ peaks. There is no evidence of magnetic peaks at $l$-even $(2n+1/4, 2n+1/4, l)$ positions (Fig. 2*c*) as observed in

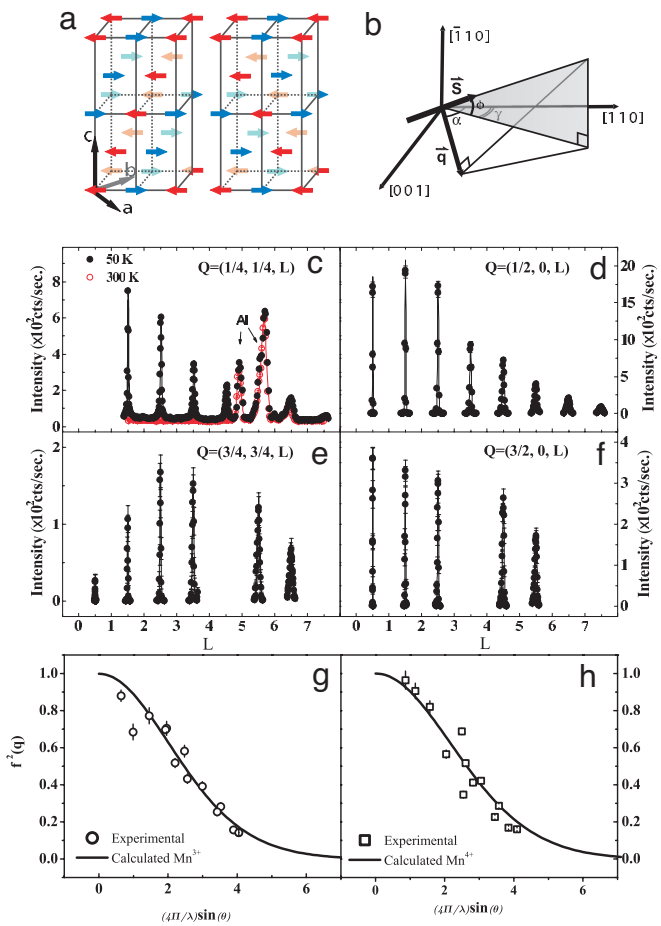


**Fig. 2.** The magnetic structure determination of PCMO. (*a*) Two possible spin arrangements for the $Mn^{3+}$ sublattice as obtained from Rietveld analysis of the HRNPD data and fits to single crystal integrated intensities at different positions. (*b*) The geometrical relationship between the $Mn^{3+}$ spin and the $MnO_2$ plane. (*c*) Scattering data along **q** = (1/4, 1/4, L) at $T$ = 50 and 300 K, respectively. (*d–f*) The $\theta - 2\theta$ scans for **q** = (3/4, 3/4, L), (1/2, 0, L), and (3/2, 0, L) that are projected to the [0, 0, L] direction. The intensities of observed magnetic peaks are fit to the generic magnetic form factor for $Mn^{3+}$ (*g*) and $Mn^{4+}$ (*h*) ions.

LSMO (11). The temperature dependence of the order parameters for the (1/4, 1/4, 3/2) (Fig. 1*c*) and (1/2, 0, 1/2) (Fig. 1*e*) peaks show that the $Mn^{3+}$ and $Mn^{4+}$ networks enter the AF long-range ordered states simultaneously at $T_N \approx 130$ K.

We measured the radial and transverse scans of all observed magnetic peaks. The product of the longitudinal peak width in full-width-half-maximum (FWHM) and the integrated intensity of the rocking curve was used as the total intensity of a Bragg peak. The observed intensity of a magnetic Bragg peak should be proportional to $I \propto |F_M(\mathbf{q})|^2/\sin(2\theta)$, where $\theta$ is the scattering angle. The magnetic structure factor $F_M$ is

$$F_M(\mathbf{q}) = \sum_j f(\mathbf{q})_j \mathbf{q} \times (M_j \times \mathbf{q}) e^{i\mathbf{q}\cdot\mathbf{r}} e^{-W_j} \qquad [1]$$

where $f(\mathbf{q})_j$, $M_j$, and $e^{-W_j}$ are the magnetic form factor, the spin moment of the $j$th ion and Debye–Waller factor, respectively.

In the case of the $Mn^{3+}$ spin network, the integrated intensities of $(2n + 1/4, 2n + 1/4, l)$ peaks depend on $\alpha$, $\phi$, and $\gamma$, where $\alpha$ is the the angle between wave vector **q** and the $MnO_2$ plane, $\phi$ is the angle between the moment direction and the [1,1,0]/[0,0,1] plane, and $\gamma$ is the angle between the projection of the spin in the [1,1,0]/[0,0,1] plane and the $MnO_2$ plane, as depicted in Fig. 2*b*. By fitting the integrated intensities of $(2n + 1/4, 2n + 1/4, l)$ peaks as a function of $\alpha$, $\phi$, and $\gamma$, we find that the best fit for the $Mn^{3+}$ form factor in Fig. 2*g* requires both $\phi$ and $\gamma$ to be zero, indicating that the $Mn^{3+}$ spins are in the $MnO_2$ basal plane and along the [1,1,0] direction (Figs. 1*a* and 2*a*). Similarly, the moment direction for $Mn^{4+}$ spins along the [1, 1, 0] direction also gives the best fit (Fig. 2*h*). Independent Rietveld analysis of the magnetic structural data on powder samples confirms that the magnetic structure has dimensions of $a_o \times 2b_o \times 2c_o$ (where $a_o$ = 5.37 Å, $b_o$ = 5.40 Å, and $c_o$ = 11.78 Å at low temperature) for the $Mn^{3+}$ magnetic sublattice and $2a_o \times 2b_o \times 2c_o$ for $Mn^{4+}$ sublattice. Although the proposed spin directions of PCMO is different from that of LSMO, where spins are aligned along the [1, 2, 0] direction in the $MnO_2$ basal plane, the presence of impurity and minority phase in LSMO makes the conclusive magnetic structural determination difficult (11).

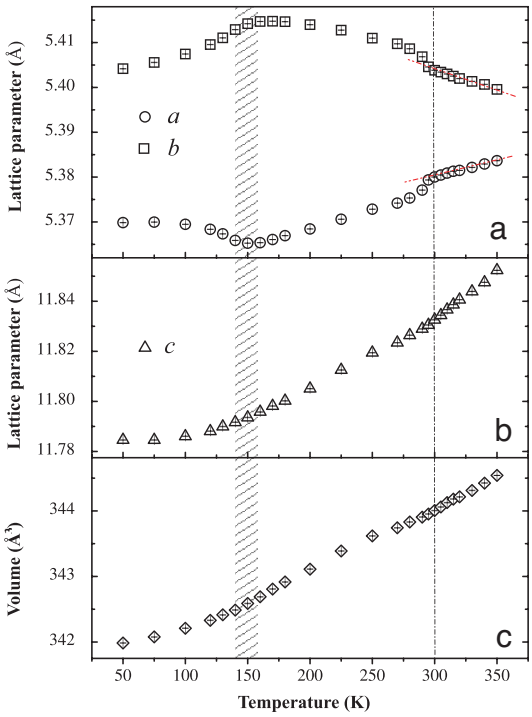


**Fig. 3.** Temperature dependence of lattice parameters and unit cell volume. The dashed line near 300 K marks the CO/OO transition temperature $T_{CO}$. Whereas the in-plane *a* and *b* lattice parameters show clear anomalies around $T_{CO}$ and $T_N$, the c-axis lattice parameter changes smoothly across both transitions. The dash-dotted lines in *a* are guides to the eye.

As PCMO is cooled from 350 K, the orthorhombicity of its structure increases with decreasing temperature and shows a clear enhancement of the orthorhombic strain around the charge ordering temperature $T_{CO}$ to accommodate the establishment of orbital ordering. Fig. 3 shows the temperature dependence of the lattice parameters and unit cell volume obtained from Rietveld analysis of the neutron powder diffraction data. Although an enhancement of the orthorhombic structure near $T_{CO}$ is expected, similar to that of other half-doped manganites (7–12), the orthorhombicity of PCMO mysteriously becomes smaller below ≈150 K, at temperatures 20 K above the $T_N$ of the system (Fig. 3). To demonstrate this more clearly, we carried out detailed studies of the (1, 1, 2) Bragg peak at temperatures 30 K < $T_N$, $T_N$ < 160 K < $T_{CO}$, and $T_{CO}$ < 320 K (Fig. 4*g*). Below $T_{CO}$, the (1, 1, 2) peak at $2\theta$ = 36.61° starts to broaden with reduced peak intensity, and then splits into two peaks [indexed as $(0, 2, 2)_O$ and $(2, 0, 2)_O$ in orthorhombic notation] at $T \approx 150$

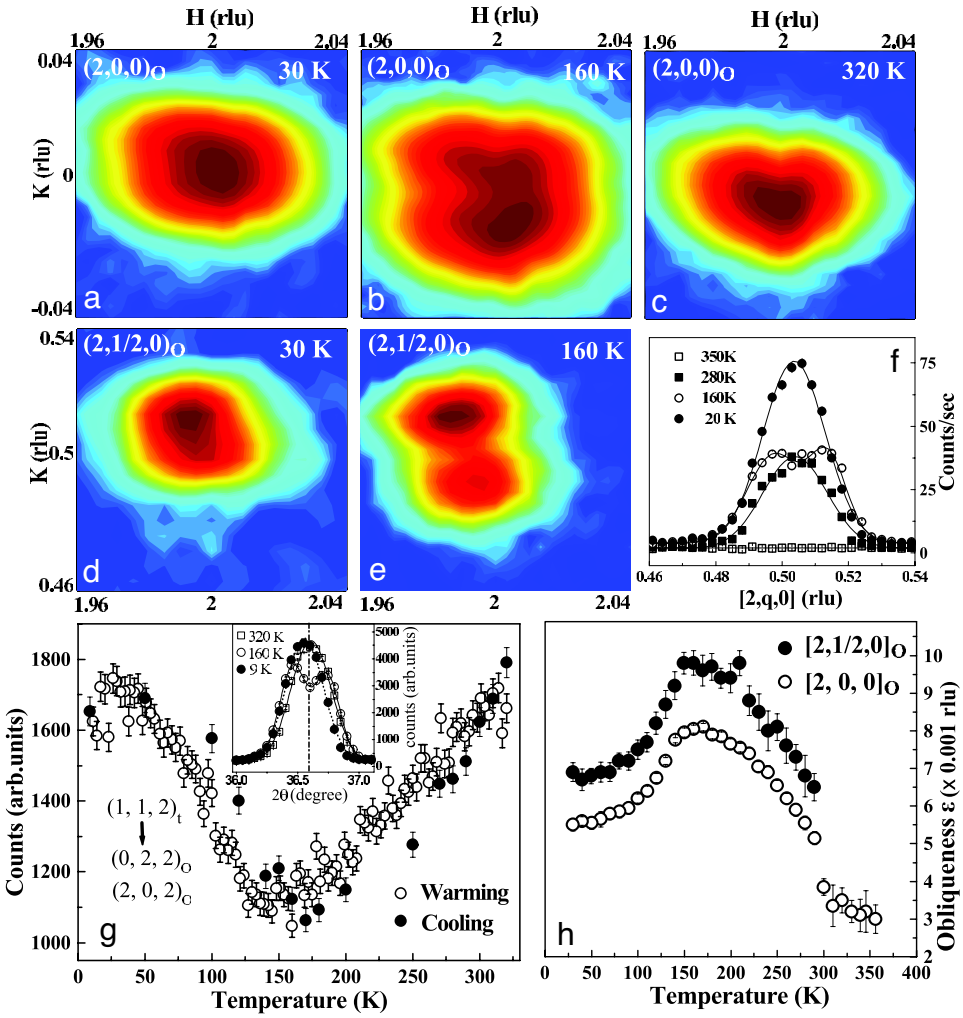


**Fig. 4.** Strong spin-lattice coupling near the magnetic transition temperature. (*a–c*) Mesh-scans around the nuclear Bragg peak $(2,0,0)_O$ (in orthorhombic notation) at $T = 30$, 160, and 320 K. (*d* and *e*) The corresponding mesh-scans around CO/OO-induced superlattice peak $(2,1/2,0)_O$ at 30 and 160 K. (*f*) Wave vector scans of the same CO/OO peak at selected temperatures. (*g*) Temperature dependence of the peak intensity from powder monitored at $2\theta = 36.61°$, which corresponds to the $(1,1,2)_t$ structural peak in tetragonal notation. (*Inset*) The splitting of the $(1,1,2)_t$ peak [the actual $(0,2,2)_O$ and $(2,0,2)_O$ in orthorhombic symmetry] becomes much more prominent at 160 K and recovers back to one peak at low temperature. (*h*) Temperature dependence of the obliqueness, the separation between the center of the split peaks in reciprocal space, for $(2,0,0)_O$ and $(2,1/2,0)_O$.

K as shown in Fig. 4*g Inset*. As the temperature continues to drop, the split peaks merge back into one at low temperature. The temperature dependence of the (1, 1, 2) peak intensity shows a continuous drop for $T < 300$ K and then the recovery below $T \approx 150$ K (Fig. 4*g*).

Fig. 4 *a–f* summarizes mesh scans in reciprocal space near the fundamental Bragg $(2,0,0)_O$ and charge ordering $(2, 1/2, 0)_O$ positions in the orthorhombic symmetry at low, intermediate, and high temperatures obtained on single crystals of PCMO. The $(2, 0, 0)_O$ peak first broadens and then splits along the transverse direction at 160 K. On further cooling to 30 K, the split peaks become one again (Fig. 4*a*). Fig. 4 *d–f* shows that the $(2, 1/2, 0)_O$ CO/OO peak, which is equivalent to the (3/4, 5/4, 0) peak in tetragonal notation, exhibits similar behavior: broadens and splits between $T_N$ and $T_{CO}$, and emerges back to one below $T_N$. To quantitatively determine the degree of orthorhombicity, we plot in Fig. 4*h* the temperature dependence of the separation between the centers of split peaks $\varepsilon$ in reciprocal space. Below $T_{CO}$ of 310 K, the distortion increases dramatically. It continues to increase and reaches its maximum around 150 K. Upon further cooling below $\approx$150 K (a temperature 20 K above $T_N$), the lattice distortion is continuously suppressed, but still remains at the lowest probed temperature of 20 K. This anomalous lattice response near $T_N$ has not been observed in LSMO or other half-doped manganite systems. In these materials, the CO/OO-induced lattice distortions do not exhibit noticeable anomalies across $T_N$ at lower temperatures (7, 8, 12). We also note that the suppression of orthorhombicity below $\approx$150 K in PCMO is not associated with the melting of charge ordering as the integrated intensity of CO peaks shown in Fig. 1 *d* and *f* display no anomalies across $T_N$. This is different from the bilayer perovskite manganites (22, 23).

The temperature dependence of AF peaks such as (1/4, 1/4, 3/2) and (1/2, 0, 1/2) shows a $T_N$ of 130 K for PCMO. Wave vector scans within the $MnO_2$ plane and along the *c*-axis (Fig. 5 *a–d*) show quite anisotropic correlations above $T_N$. Scans along the [*h, h,* 1/2] and [*h,* 0, 1/2] directions in the $MnO_2$ plane display the clear presence of two-dimensional short-range spin correlations above $T_N$. Fig. 5*a* suggests that the in-plane $Mn^{3+}$–$Mn^{3+}$ spin correlations are established at temperatures as high as 210 K, whereas the interplane $Mn^{3+}$–$Mn^{3+}$ spin correlations are turned on only below $T_N$ (Fig. 5*c*). The spin correlations between $Mn^{4+}$ ions behave similarly as shown in Figs. 5*b* and 4*d*. The short-range AF spin correlations have been fit to a Lorentzian line

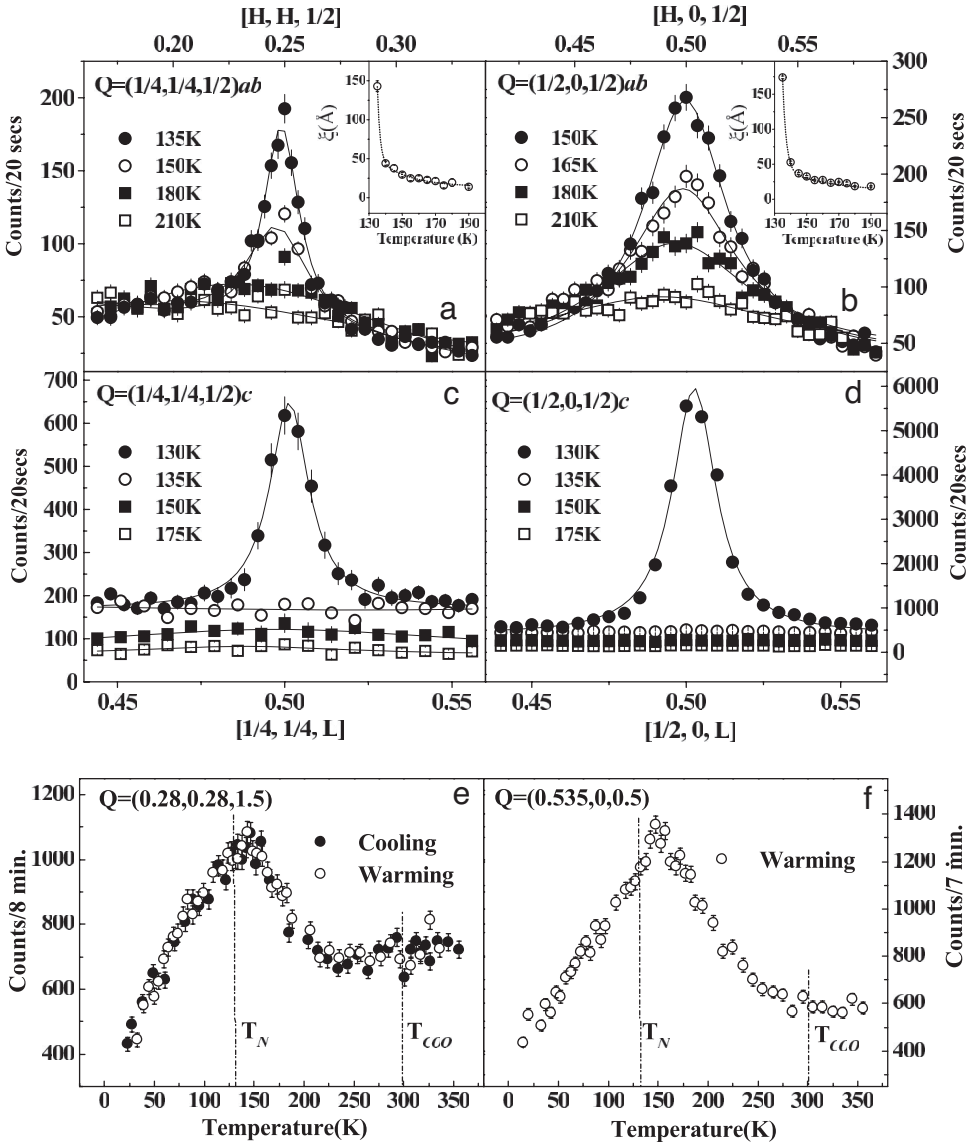


**Fig. 5.** Crossover from two-dimensional AF fluctuations to three-dimensional AF order. Wave vector scans of AF scattering from the $Mn^{3+}$ sublattice near **q** = (1/4, 1/4, 1/2) within Mn-O plane (*a*) and along the interplane (*c*) direction. Similar scans from the $Mn^{4+}$ sublattice near (1/2, 0, 1/2) are presented in *b* and *d*. (*Insets*) The evolution of magnetic correlation lengths above the long range AF order temperature $T_N$ = 130 K. (*a* and *f*) Temperature profiles of short-range magnetic scattering measured at **q** = (0.28, 0.28, 3/2) (*e*) and **q** = (0.535, 0, 1/2) (*f*). Those wave vectors have been chosen to avoid the contamination from the magnetic Bragg peaks.

shape as shown in the solid curves in Fig. 5 *a* and *b*. Their linewidths decrease with decreasing temperature. Below $T_N$, the Lorentzian line shape is gradually taken over by a Gaussian component indicating the development of long-range AF order. Fig. 5 *a* and *b Insets* show the temperature dependence of the in-plane spin–spin correlation lengths. Although the correlation lengths clearly diverge near $T_N$ as expected with the establishment of the long-range AF order, there is no anomaly around ≈150 K.

One way to determine the temperature dependence of the staggered magnetic susceptibility is to track the scattering intensity at a wavevector position slightly away from the magnetic Bragg peak (to avoid the Gaussian component) but close enough to probe short range spin–spin correlations. In a standard second–order AF phase transition, one would expect the staggered susceptibility to increase with decreasing temperature, peak at the transition temperature, and then decrease below $T_N$. Fig. 5 *e* and *f* shows the temperature dependence of the scattering intensity at (0.28, 0.28, 3/2) and (0.535, 0, 1/2), which probe the $Mn^{3+}$ and $Mn^{4+}$ spin–spin correlations, respectively. The susceptibilities corresponding to $Mn^{3+}$ and $Mn^{4+}$ spin correlations start to increase around 240 K. They reach their maxima at ≈150 K on cooling and are continuously suppressed below $T$ ≈150 K, showing no anomaly across $T_N$. Currently, we do not understand why there is no anomaly in the spin correlation lengths at 150 K (see Fig. 4 *a* and *b Insets*).

## Discussion and Conclusion

In general, CO/OO ordering is strongly coupled to the lattice, has a large energy scale, and occurs at higher temperatures than magnetic ordering. As a consequence, the development of magnetic order at low temperature usually has no effect on the lattice distortions induced by the CO/OO order. For previously studied half-doped manganites (7–12), orbital ordering is always established simultaneously with charge ordering (18, 19). In addition, the CE-type AF order occurring at low temperatures

stabilizes the CO/OO ordered phase and the orthorhombicity of the system saturates below $T_N$ (7). Because PCMO has a smaller $A_{0.5}A'_{1.5}$ ionic radius and larger lattice distortion than that of LSMO, one would expect CO/OO order in PCMO to be more robust than the magnetic order. Instead, the dramatic reduction of the orthorhombicity near $T_N$ indicates a strong spin-lattice coupling that can influence the distortion already established by CO/OO ordering. At present, it is unclear why PCMO should behave differently from other half-doped manganites. Perhaps the small Pr/Ca ionic sizes and large lattice distortion in this material can enhance the CE-type AF superexchange interaction and make it comparable to the energy of CO/OO ordering. For LSMO, inelastic neutron scattering experiments (24) have shown that the ferromagnetic exchange coupling along the zigzag chain direction (see Fig. *1a*) is ≈5.5 times larger than that of AF exchange in between the chains ($J_{FM}/J_{AF}$ = 9.98 meV/1.83 meV ≈ 5.5).

In the case of PCMO, our preliminary spin wave measurements based on the Hamiltonian similar to that reported in ref. 24 suggest that this ratio becomes $J_{FM}/J_{AF}$ = 8.7 meV/6.5 meV ≈ 1.34. Therefore, the AF exchange interaction is much stronger in PCMO than in LSMO, making a more robust AF CE structure with little anisotropy between *a* and *b* axis directions. This means that the AF order in PCMO prefers a tetragonal structure rather than orthorhombic (5), and provides a competing energy scale to the already established CO/OO ordering. In any case, our data clearly indicate that the magnetic exchange energy in PCMO is an important competing force and must be taken into account to understand its low temperature electronic properties. Furthermore, the spin-lattice coupling in PCMO is much stronger than that for other half-doped manganites.

In summary, we have carried out neutron scattering studies of the lattice and magnetic structure of the layered half-doped manganite PCMO. The system first displays CO/OO order and then develops CE-type AF order at low temperatures. We have discovered that AF order can have a large effect on the already established lattice distortions induced by the CO/OO. This result indicates a strong spin-lattice coupling in PCMO. It also contrasts with all other known half-doped manganites, where AF order has little or no influence on orthohombic strains in the system. We argue that the reason for this difference is that magnetic exchange coupling in PCMO is much more isotropic, favoring a tetragonal AF crystal structure. As a consequence, the low-temperature electronic properties of the half-doped manganites are determined not only by CO/OO ordering, but are also affect by strong spin-lattice coupling.

## Materials and Methods

We grew single crystals of PCMO using the traveling solvent floating zone technique. High resolution neutron powder diffraction (HRNPD) experiments were carried out on BT-1 at the NIST Center for Neutron Research (NCNR) with powder of crushed single crystals. Elastic neutron scattering measurements were carried out on the thermal triple-axis instruments BT-7 and BT-9 at NCNR. Rietveld analysis on the powder data indicates that the crystals were single phase without detectable impurities. The crystals were mounted in a closed cycle He displex and aligned in successive orientations to allow the wavevectors in the form of (*h, h, l*), (*h, k,* 0) and (*h,* 0, *l*) accessible in the horizontal scattering plane. Neutron energies of 14.7 meV and 13.7 meV were used with pyrolytic graphite crystals as monochromator, analyzer, and filters.

We thank D. Khomskii for helpful discussions. The work was supported by National Science Foundation Grant DMR0453804. Oak Ridge National Laboratory is managed by UT-Battelle, LLC, for the U.S. Department of Energy under Contract DE-AC-05-00OR22725. This work was also performed under the U.S.–Japan Cooperative Program on Neutron Scattering.

1. Imada M, Fujimori A, Tokura Y (1998) *Rev Mod Phys* 70:1039–1263.
2. Tranquada JM, Sternlieb BJ, Axe JD, Nakamura Y, Uchida S (1995) *Nature* 375:561–563.
3. Fujita M, Goka G, Yamada K, Tranquada JM, Regnault LP (2004) *Phys Rev B* 70:104517.
4. Wollan EO, Koehler WC (1955) *Phys Rev* 100:545–563.
5. Goodenough JB (1955) *Phys Rev* 100:564–573.
6. Dai P, Zhang J, Mook HA, Liou S-H, Dowben PA, Plummer EW (1996) *Phys Rev B* 54:3694–3697.
7. Radaelli PG, Cox DE, Marezio M, Cheong S-W (1997) *Phys Rev B* 55:3015–3023.
8. Jirak Z, Krupicka S, Simsa Z, Dlouha M, Vratislav S (1985) *J Magn Magn Mater* 53:153–166.
9. Daoud-Aladine A, Rodriguez-Carvajal J, Pinsard-Gaudart L, Fernandez-Diaz MT, Revcolevschi A (2002) *Phys Rev Lett* 89:097205.
10. Ye F, Fernandez-Baca JA, Dai P, Lynn JW, Kawano-Furukawa H, Yoshizawa H, Tomioka Y, Tokura Y (2005) *Phys Rev B* 72:212404.
11. Sternlieb BJ, Hill JP, Wildgruber UC, Luke GM, Nachumi B, Moritomo Y, Tokura Y (1996) *Phys Rev Lett* 76:2169–2172.
12. Larochelle S, Mehta A, Lu L, Mang PK, Vajk OP, Kaneko N, Lynn JW, Zhou L, Greven M (2005) *Phys Rev B* 71:024435.
13. Solovyev IV, Terakura K (1999) *Phys Rev Lett* 83:2825–2828.
14. van den Brink J, Khaliullin G, Khomskii D (1999) *Phys Rev Lett* 83:5118– 5121.
15. Yunoki S, Hotta T, Dagotto E (2000) *Phys Rev Lett* 84:3714–3717.
16. Mutou T, Kontani H (1999) *Phys Rev Lett* 83:3685–3688.
17. Khomskii D, van den Brink J (2000) *Phys Rev Lett* 85:3329–3329.
18. Murakami Y, Kawada H, Kawata H, Tanaka M, Arima T, Moritomo Y, Tokura Y (1998) *Phys Rev Lett* 80:1932–1935.
19. Dhesi SS, Mirone A, De Nadai C, Ohresser P, Bencok P, Brookes NB, Reutler P, Revcolevschi A, Ragliaferri A, Toulemonde O, van der Laan G (2004) *Phys Rev Lett* 92:056403.
20. Tokura Y (2006) *Rep Prog Phys* 69:797–851.
21. Ibarra M, Retoux R, Hervieu M, Autret C, Maignan A, Martin C, Raveau B (2003) *J Solid State Chem* 170:361–367.
22. Kimura T, Kumai R, Tokura Y, Li JQ, Matsui Y (1998) *Phys Rev B* 58:11081–11084.
23. Argyriou DN, Bordallo HN, Campbell BJ, Cheetham AK, Cox DE, Gardner JS, Hanif K, dos Santos A, Strouse GF (2000) *Phys Rev B* 61:15269–15276.
24. Senff D, Krüger F, Scheidl S, Benomar M, Sidis Y, Demmel F, Braden M (2006) *Phys Rev Lett* 96:257201.
25. Mathieu R, He JP, Yu XZ, Kaneko Y, Uchida M, Lee YS, Arima T, Asamitsu A, Tokura Y (2007) con-mat/070119.